Rate-Limiting Processes in the Formation of Single-Wall Carbon Nanotubes: Pointing the Way to the Nanotube Formation Mechanism

O. Jost,*,† A. A. Gorbunov,† J. Möller,† W. Pompe,† X. Liu,‡ P. Georgi,‡ L. Dunsch,‡ M. S. Golden,‡ and J. Fink‡

Institute of Materials Science, Dresden University of Technology, D-01062 Dresden, Germany, and Institute for Solid State Research, IFW Dresden, P.O. Box 270016, D-01171 Dresden, Germany

Received: August 10, 2001; In Final Form: January 14, 2002

Four rate-limiting processes for the formation of single-wall carbon nanotubes (SWCNT) could be identified by varying furnace temperature, gas type, and pressure in a pulsed-laser evaporation setup. One rate-limiting process accounts essentially for all relevant gas-pressure dependencies and can be quantitatively described using a single gas-specific constant. One thermally activated process is related to fullerene formation, whereas another process, following a T^2-law, is discussed in terms of the diffusion of carbon through molten catalyst nanoparticles. The data provide strong support for an "undercooled melt" mechanism of nanotube formation.

1. Introduction

Carbon nanotubes are the focus of intense interest worldwide because of their outstanding properties.[1,2] Since the experimental discovery of single-wall carbon nano-tubes (SWCNT), a number of methods for the production of SWCNT have been developed, like those involving the catalytic decomposition of carbon-containing compounds or evaporation-related approaches. A recent review of the different SWCNT production approaches can be found in ref 3. Although there is a growing number of reports describing the influence of variations of individual SWCNT synthesis variables, the relevant processes determining the SWCNT nucleation and growth conditions are still not known. This fact is due, at least in part, to the large number of partially interconnected process variables. Very recently, substantial progress could be achieved as regards the evaporation-based SWCNT production methods. It could be shown that the SWCNT formation process is a condensed phase process in a completely thermalized environment, occurring on a time scale of milliseconds to seconds.[4−6] The existence of catalyst particles exceeding a minimum size was found to be necessary for SWCNT formation to start.[7] As now some basic boundary conditions for the formation of SWCNT are established or at least confined (especially the time scale), the next step would consequently involve the exploration of rate-limiting processes in the formation of nanotubes. The identification of such SWCNT formation rate-limiting processes is the aim of this work.

Primary synthesis variables of significance for the exploration of rate-limiting processes in gaseous environments are obviously the gas pressure, environment temperature and time allowed for SWCNT formation. Recent results for different SWCNT production methods following the evaporation approach could show that the nanotube abundance strongly depends on these synthesis parameters.[8−14] Here, we focus on the exploration of *combined* gas type, gas pressure, and temperature dependencies of the SWCNT formation. For the nanotube production, we have used the pulsed laser evaporation approach. Compared to evaporation techniques based on the continuous vaporization of a carbon source, this method has the advantage that the environment temperature can be varied in a more controlled manner. For the characterization of the produced SWCNT soot, we primarily used a method based on optical absorption spectroscopy (OAS). This characterization method, first reported for SWCNT in ref 15, is based on the excitation spectrum of SWCNT[16] and allows the simultaneous determination of SWCNT diameter and yield.[17]

2. Experimental Section

The conditions given below were used as standard conditions. The target materials (charcoal, Co, and Ni) had a purity of >99.97%. The dry powders were milled in the desired mixing ratio, the total catalyst content being 1.5 at % with the catalyst composition $Co_{0.5}Ni_{0.5}$}. One gram of material was then pressed into a dense pellet of 13 mm in diameter. Freshly prepared targets were cured (with a ramp of 100 °C/h to 1150 °C and then held for 4h in $\approx 10^3$ Pa Ar) prior to the first usage. A Q-switched Nd:YAP laser (wavelength 1.08 μm, pulse duration 20 ns, pulse energy 700 mJ) was used to irradiate the center of the flat target surface with a pulse rate of 15 Hz and a total number of laser pulses of ≈1800 per run. All pulses were directed into the same spot, leading to a pitted evaporation zone with a circular area of around 16−20 mm^2 and a maximum depth <1. One laser pulse evaporated around 1.5×10^{17} atoms.

The target was placed in a quartz-glass tube with an inner diameter of 17 mm inside a resistance-heated tube furnace with a heated length of 200 mm. The tube-wall temperature, determined with thermocouples in the center of the furnace was held constant at 1150 °C, with a maximal deviation of about ±10 °C. The high-temperature zone (i.e., that with at least 97% of the maximum temperature) extended over ≈50−60 mm along the glass tube along either side of the center of the furnace. Nitrogen was used as the standard carrier gas to transport the evaporation products downstream of the target. No reactive influence of nitrogen on the SWCNT formation process was observed, in keeping what has been reported previously.[18] The pressure of the carrier gas was kept constant at a value of 60 kPa. A gas flow peak velocity of ≈2 cm/s was used, obtained

* Corresponding author. Fax: +49-351-463-1422. E-mail: jost@tmfs.mpgfk.tu-dresden.de.
† Institute of Materials Science.
‡ Institute for Solid State Research.

10.1021/jp013138s CCC: $22.00
Published on Web 02/19/2002

by correcting the applied flow rate for the working pressure and measured tube-wall temperature in the center of the furnace. Both the target and a water-cooled copper collector were positioned in the hot zone of the furnace located 30 mm and 60 mm behind the center of the furnace, respectively. The soot produced after irradiation of the target was carried away by the gas and deposited almost exclusively on the collector, thus enabling a representative quantification of the SWCNT abundance. The collector temperature could be maintained near room temperature thus resulting in a quenching effect, that is assumed to stop any ongoing reactions in the soot. This is necessary, as it is known that the SWCNT formation process can extend up to seconds.[4] The quenching, together with a nearly constant gas flow velocity in the hot zone of the furnace, i.e., constant time-of-flight of the SWCNT soot, enabled us to keep the time window allowed for SWCNT growth processes fairly *constant*. In addition, if the soot were allowed to slowly propagate through the temperature gradient from the hot zone to the end of the furnace tube (i.e., no quenching, with ongoing SWCNT formation during this propagation), a reliable determination of the role played by the hot zone temperature would not be possible.

After every run, the collected soot was characterized. Besides transmission electron microscopy (TEM) observations (with a Philips CM-200) on soot in the as-produced state, optical absorption spectroscopy (OAS) was used. Details of the OAS measurement and sample preparation can be found in ref 17. Three pronounced absorption bands are visible in OAS spectra of SWCNT-containing material, reflecting interband transitions between the van Hove singularities in the electronic structure of the SWCNT.[15] The most pronounced SWCNT absorption band can be used as a measure for the overall abundance[17] after three background correction steps. First the optical density values of the whole spectrum were scaled for different background intensities by using one optical density value between the SWCNT peaks (at 1.05 eV, the optical density value at this position was always kept below 0.08) as a normalization reference. This was followed by a simple linear subtraction of the background under the chosen peak. It has to be mentioned at this point that we observed that the SWCNT peak intensity does not scale linearly with the thickness of the soot film. The deviation was found to be as large as 15% for optical densities differing by a factor of 2. This effect could also lead to the loss of the SWCNT absorption bands for extremely thick films (buckypaper-like material for example). Thus, the film thickness (represented by the optical density value of the background at a reference position in the spectrum) had to be kept as *constant as possible* for all measurements in order to get reliable results from the SWCNT yield determination procedure (see below). Nevertheless, as it was not possible to control the film-thickness always to the required extent, we applied an additional correction to account for SWCNT peak intensity differences resulting from *small* deviations from the targeted film-thickness. For this, a number of calibration samples were prepared from the same SWCNT containing soot with different background optical density values (i.e., slightly different film thicknesses) resulting in a scaling expression for the SWCNT peak intensity.

The width of the peak is a function of the diameter distribution of SWCNT.[17] The area below the peak is then a measure for the integral of the optical absorption coefficient of all contributing SWCNT of different diameter. In this way the determined peak area is essentially proportional to the SWCNT abundance and can consequently be used as an express semiquantitative indicator of the SWCNT yield.[17] The SWCNT peak area of nanotube soot produced under the standard synthesis conditions described above (approximately 40% nanotube content from TEM observations) is assigned a relative abundance value A of $A = 1$. If not otherwise stated, all abundance values in this work are given relative to this standard value of A. To determine the total experimental reproducibility, soot material from different soot production runs under the standard synthesis conditions were investigated. The area of the SWCNT peak determined after the correction procedure did not deviate by more than $|\Delta A| = 0.05$ on the relative abundance scale.

3. Results and Discussion

One can assume the overall SWCNT formation process to be one depending on a number of sub-processes running in series or parallel, with the SWCNT being the end-product. The slowest sub-processes would form a critical reaction path. They are rate-limiting, and thus determine in the end the observed SWCNT abundance. These should be extractable from the experimental data. In the following, four rate-limiting processes (which will henceforth be labeled using the Roman numbers I, II, III, and IV)) are described and discussed.

3.1. Gas Kinetic Process I. Figure 1a shows the pressure dependence of the SWCNT abundance for the three gases nitrogen, helium and argon at 1150 °C and for nitrogen and argon at 950 °C. All gases show low abundances for comparatively low pressures with a relatively sharp low pressure limit, below which no SWCNT could be detected. Pressure maxima of the abundance are found for the two gases argon and nitrogen, the argon pressure maxima being located at slightly higher pressures. As Figure 1a indicates, helium also shows a pressure-related SWCNT abundance dependence, but the abundance values are significantly shifted to higher pressure with respect to the other two gases with no distinct abundance maximum being observable in the investigated pressure range.

The gas type, pressure, and temperature of a gas determine the conditions for momentum transfer, heat diffusion and mass diffusion within this gas which—as only the gas kinetic variables are known—is best expressed by a universal gas kinetic coefficient D^g:

$$D^g = \frac{\bar{c}\lambda}{3} \qquad \text{with} \qquad \bar{c} = \sqrt{\frac{3RT}{M}} \qquad \text{and} \qquad \lambda = \frac{RT}{\sqrt{2}pd^2N_A\pi} \quad (1)$$

(temperature T, root-mean-square gas molecule velocity $\bar{c}$, molecular mass of the gas molecules M, mean free path of the gas molecules λ, Avogadro number N_A, gas constant R, pressure p, and the gas molecule diameter d). Equation 1 can be rewritten in terms of the three variables T, p, and the gas-specific constant σ_M varied here:

$$D^g = k\frac{T^{3/2}}{p\sigma_M} \qquad \text{with} \qquad \sigma_M = d^2\sqrt{M} \qquad \text{and} \qquad k = \frac{R^{3/2}}{\sqrt{6}\pi N_A} \quad (2)$$

It turned out that the data shown in Figure 1a coincide in a reasonably good manner with variations of D^g for the three gases helium, argon, and nitrogen. This is shown in Figure 1b. This indicates that indeed the SWCNT abundance development is bound to variations in the transport conditions in these gases. As such, this gas kinetic process acts as formation rate-limiting at some point in the chain of processes leading to SWCNT

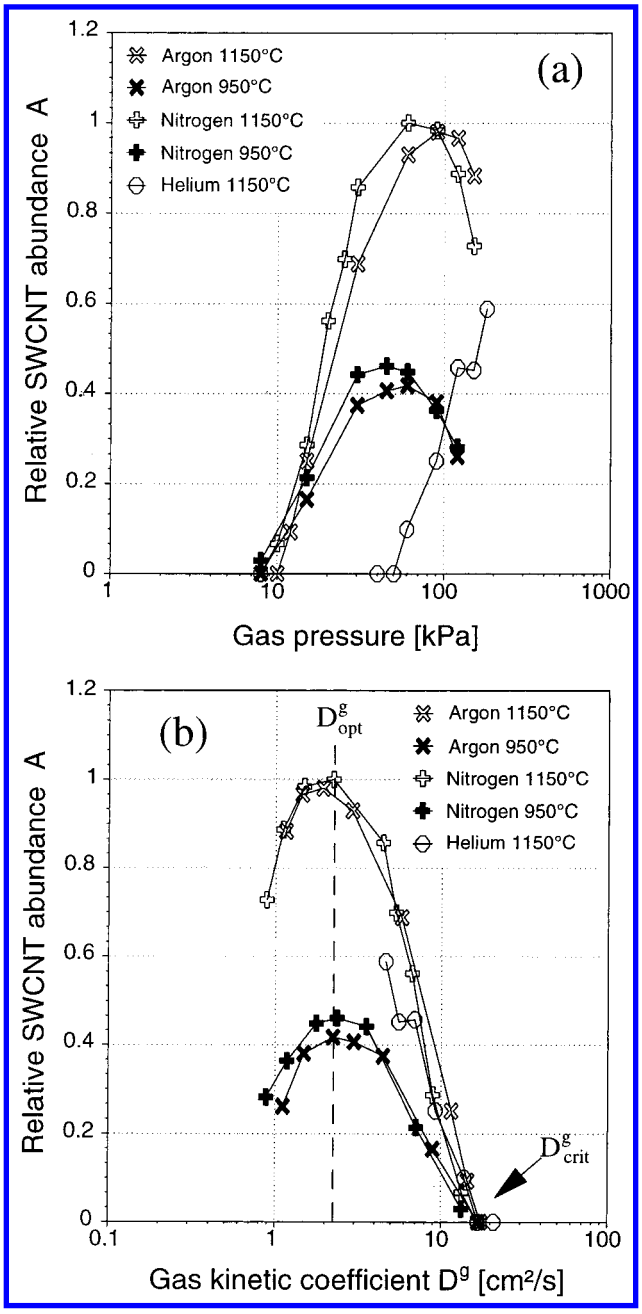

Figure 1. Dependence of the relative SWCNT abundance, *A*, on the three gases argon, nitrogen and helium at different temperatures (a) as functions of gas pressure and (b) versus the change in the respective gas kinetic coefficients. For details see text.

formation. The data in Figure 1b show a distinct upper limit D^g_{crit} 15−20 cm²/s for the formation of SWCNT and also clearly show D^g_{opt} 1.5−3 cm²/s to be optimal for the abundant formation of SWCNT. There is also a decay of the abundance for $D^g < D^g_{opt}$, which may point to a lower limit of D^g.

These data indicate clearly that for a wide range of process conditions, the observed SWCNT formation limit and abundance optimum can be maintained by keeping the respective ratio $T^{3/2}$ to p in the furnace constant. Following this as a guide, we can expect a yield maximum with helium as carrier gas for p = 400−450 kPa at a temperature of 1150 °C. The gas-type dependence of the SWCNT abundance for the gas kinetic process under consideration is completely described by the gas-specific constant σ_M. For comparison, σ_M is tabulated in Table 1 for some common gases which are considered to be chemically inactive in the SWCNT formation process.

TABLE 1: Gas-specific Constant $\sigma_M = \sqrt{M}\, d^2$

gas	$\sigma_M \left[10^{-21} \frac{m^2\, kg^{1/2}}{mol^{1/2}}\right]$
nitrogen	20.85
helium	3.35
neon	9.49
argon	16.58
krypton	28.54
xenon	42.38

The existence of one D^g_{opt} value points to unique optimum transport conditions which remain the same for different gases. So, the comparison of the results above with published results for other SWCNT synthesis methods employing arc-discharge and a continuous-wave laser might be useful in order to find similarities. For the continuous-wave laser synthesis of SWCNT (without an external furnace around the target),[19] the optimum conditions for the SWCNT synthesis were found to be between 25 and 50 kPa for both argon and nitrogen, whereas in helium gas traces of SWCNT could be found only close to the upper limit of the applied pressure variations of 67 kPa which was attributed to a faster quenching of the evaporated material in helium.[20] There are also results for the arc-discharge method. The pressure ratio for optimum SWCNT abundances by comparing the gases helium and argon has values of p_{opt}(He)/p_{opt}(Ar) ≈ 6.6[12] which fits reasonable well with the ratio of the relevant gas-type parameters σ_M(Ar)/σ_M(He) ≈ 5 as derivable from Table 1 (see also eq 2). This implies that there might be similar gas kinetic processes active in the arc-discharge method. On the other hand, the absolute pressures leading to optimum abundances are found to be around 10 kPa in the case of argon and 50−70 kPa in the case of helium, both values being a factor of roughly 5−7 smaller than those for the pulsed laser evaporation process. The reason for these differences between the different methods is unclear and can only be speculated about at this stage. One of the major differences between the two methods is the quenching conditions of the evaporated material, with the thermal gradient expected to be steeper after an evaporation pulse than during a continuous evaporation. On the other hand, a small gas pressure in the arc-discharge method results in a small backpressure effect (the gas pressure controls the buffer effect against the plume expansion) for expanding evaporation clouds which should result, from thermodynamic considerations, again in a sharper quenching effect for the now faster expanding condensation cloud. Thus, the thermal quenching conditions for optimal SWCNT abundance might be similar for both methods. The question then arises as to why the quenching velocity should be so important for obtaining a high SWCNT yield? This question has to be asked, as it is now agreed[4−6] that the SWCNT formation itself takes place on the time scale of milliseconds to seconds, which does not fit with the time scale of the quenching process. The answer might be that the quenching velocity determines the formation probability of suitable carbonaceous precursors for the SWCNT formation.

In contrast to D^g_{opt}, the existence of a D^g_{crit} value indicates an exclusion condition for the formation of SWCNT. One possibly related observation is that at $D^g \gg D^g_{opt}$ the collected quantity (i.e., not just SWCNT but total soot) decreased significantly, which has also been reported previously at low gas pressures.[14] Such considerations led us to determine the soot collection limit, which we found to be at around 5 kPa for argon and nitrogen and at around 30 kPa for helium. This pressure ratio of p(He)/p(Ar) ≈ 6 also fits reasonably well with the ratio of the relevant gas-type parameters σ_M(Ar)/σ_M(He) ≈ 5 as derived from Table

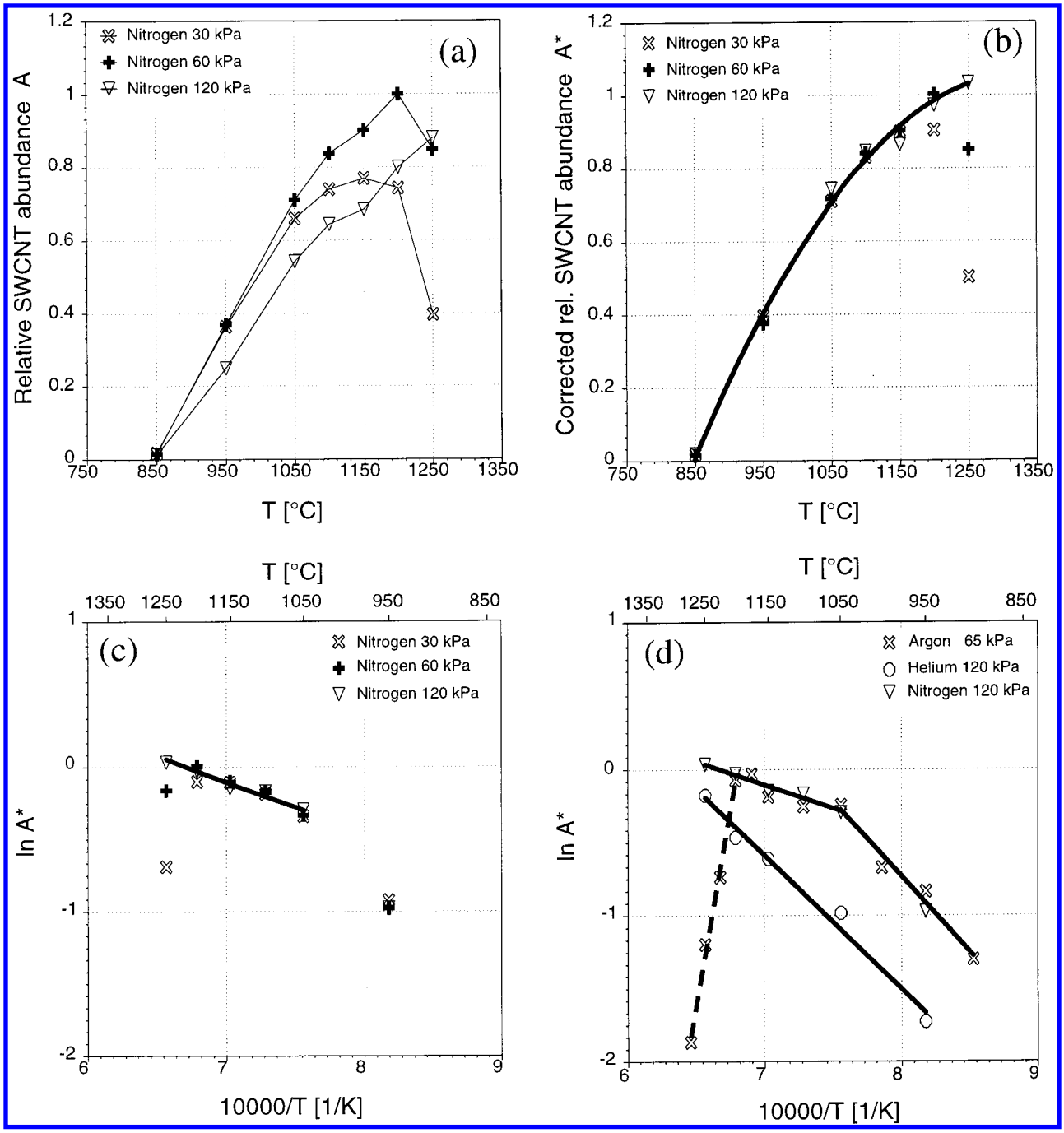

Figure 2. Temperature dependence of the relative SWCNT abundance, *A*, for different nitrogen pressures (a) without and (b) with compensation for the gas-kinetic process described as process I in the text. The values from (b) are also shown in an Arrhenius-type plot in (c). Analogous to (c) is (d) an Arrhenius-type plot for the gases argon, helium and nitrogen. The thicker solid lines in (b), (c), and (d) are trend lines.

1. Our TEM observations of soot obtained for the low pressure regime revealed that the soot contained only a small amount of carbonaceous species but a high concentration of graphite-covered metal catalyst particles. As the weight loss of the target remained nearly constant, the question now is, where did all the evaporated carbon go? The most probable answer to this question is that the quenching proceeds too fast to allow (more or less amorphous) carbonaceous units to grow to a significant size. Thus, a very high proportion of small carbon fragments (too small to become "condensed") might diffuse away. These very small carbon fragments seem to be unsuitable for the SWCNT nucleation and/or growth otherwise a significant SWCNT concentration should be observable. Thus, there might be a lower size-limit for carbonaceous material to become a suitable precursor for the SWCNT formation. On the other hand, an optimum number of carbonaceous units of the correct size would mean optimum SWCNT abundance. This would fit to the speculation given in the last paragraph that the quenching velocity determines the formation probability of suitable precursors for the SWCNT formation. Nevertheless, this concept of a quenching-velocity controlled size of carbonaceous units for SWCNT formation does not provide any useful information as to which carbon unit size or size distribution would be the suitable one.

3.2. Further Rate-limiting Processes II−IV. *3.2.1. Determination Procedure.* In Figure 2a, the general dependence of the SWCNT abundance on the furnace wall temperature for different nitrogen pressures is shown, as obtained from OAS data. As follows from eq 2 and Figure 1b, each data point is associated with a particular value of D^g of which the effect on

the SWCNT abundance is known. Thus, on the basis of Figure 1b, we can scale the yield data in Figure 2a to account for differences originating from different D^g values. A D^g reference value of $D^g = 2.3$ cm^2/s has been chosen for this compensation (a value close to D^g_{opt}). The corrected SWCNT abundance A^*, compensated for differences in the D^g values, is shown in Figure 2b. A SWCNT formation limit is observable in Figure 2b for temperatures at $\approx$ 850 °C consistent with data reported previously.[9] For the temperature range above 850 °C up to the temperature of the abundance maximum, the abundance increases monotonically in each case. As is obvious from Figure 2b, the compensation procedure in this temperature range completely accounts for the pressure dependence of the SWCNT abundance. This means that, except for the gas-kinetic process described as process I in the previous section *all* the major contributing sub-processes in the formation of SWCNT are pressure independent up to the temperature of the respective abundance maximum. This, in turn, also means that *all the other processes* contributing to the SWCNT formation, whether rate-limiting or not, *are purely based on condensed phases*. This is true at temperatures up to the respective abundance maxima. The abundance maxima in Figure 2b are, on the other hand, slightly temperature and pressure dependent. The abundance maxima are accompanied by an abundance decrease for further increasing temperature.

Figure 2c shows an Arrhenius plot of the data from Figure 2b. A corresponding Arrhenius plot for variations of the gas type is shown in Figure 2d. Values below $A^* < -2$ are not displayed in both figures as they lie below the experimental reproducibility in $|\Delta A|$ of 0.05. The data in Figure 2c,d show some similiarities except for the helium related values. Roughly three groups (II−IV) of rate-limiting processes which may share a common origin can be derived from the data shown in Figure 2c,d.

(II) The nitrogen data in Figure 2c seem to indicate a thermally activated process plotted as a linear trend line with an Arrhenius activation energy of $E_a \approx 30-40$ kJ/mol. Roughly the same E_a is derivable from the argon data in Figure 2d.

(III) In Figure 2d, for helium over the whole temperature range investigated and for argon and nitrogen at temperatures below 1050 °C, another thermally activated process with a higher activation energy seems to dominate. The corresponding $E_a \approx 70-90$ kJ/mol. The helium-related data also show a temperature shift compared to argon and nitrogen.

(IV) For the argon- and nitrogen-related data in Figure 2c,d, abundance maxima are observable, followed by a decrease at higher temperature. For the argon data in Figure 2d this is indicated by a dashed trend line.

In the following, we deal with each of the remaining rate determining processes in turn. Our discussion is organized in order of increasing temperature.

3.2.2. Discussion of the Thermally Activated Process (III) with $E_a \approx 70-90$ kJ/mol. The available data allow a comparison with published results for the pulsed laser evaporation approach with argon as carrier gas. For the evaporation of catalyst doped graphite targets (using laser pulses with pulse duration on the nano-second scale), the formation of SWCNT has never been reported for furnace environment temperatures significantly below 800 °C. Nevertheless, it could be shown that the abundant formation of SWCNT in the pulsed laser evaporation approach becomes possible at temperatures far below 800 °C by exchanging the graphite in the targets by fullerenes (C_{60}).[21] This suggests that the SWCNT formation depends on the presence of fullerenes in some way.

From ref 22, the activation energies for the formation of higher fullerenes ($C_{76}-C_{96}$) increases with fullerene size and amounts to $\approx$70−85 kJ/mol, whereas the activation energies for C_{60} and C_{70} formation are $\approx$55−60 kJ/mol. Furthermore, for the pulsed laser evaporation process, it has been reported that a substantial quantity of these higher fullerenes form for temperatures above 600−800 °C with a saturation occurring at temperatures above 1000 °C.[22] All of these reported results are in good agreement with the thermally activated process which shows up from the argon and nitrogen data here at temperatures below 1050 °C. Thus it appears reasonable to assign fullerene formation to the thermally activated process denoted process III above.

Published data can also provide a possible explanation for the shift of the helium data toward higher temperatures in Figure 2d, as, from the value of the activation energy, they might also be considered to reflect the fullerene formation process. Direct spectroscopic observations of the evaporation cloud for the pulsed laser evaporation of graphite[23] in combination with an analysis of the fullerene content of the produced soot have revealed that the fullerene formation process begins during the quenching process of the gas plume. For low furnace temperatures (temperatures below 600 °C), only small traces of fullerenes could be found which was attributed to a too rapid quenching in this cool environment, which effectively suppressed the fullerene nucleation (the temperature window for fullerene formation was passed through too fast). The fullerene formation process itself was found to be exothermic. In this context, it should be mentioned that the carrier gases helium, argon and nitrogen have different thermal conductivities, with the thermal conductivity of helium being eight times higher than those of nitrogen and argon. Thus, quenching in helium can proceed faster than in argon and nitrogen and the heat released in the exothermic nucleation of fullerenes can be distributed more efficiently. In helium, this finally results in an overly rapid quenching in the fullerene formation environment and in a too fast passing through the temperature window of fullerene formation, thus suppressing the further fullerene nucleation. As a consequence, higher furnace temperatures are required when using helium as a carrier gas to get a fullerene yield comparable to that in argon and nitrogen. One additional remark should be added to the discussion above. TEM images show no SWCNT in the soot for temperatures of 800 °C and below. For temperatures slightly above this limit and for nearly ideal gas kinetic process conditions, we found traces of SWCNT separated as well as bundled, but these nanotubes had lengths of up to hundreds of nm, indicating relatively suitable growth conditions for the nucleated SWCNT. No short, sea-urchin type SWCNT could be observed. Similar results have been reported previously.[21] These results imply that the nucleation or nucleation density of SWCNT will be affected by the thermally activated process having an $E_a \approx 70-90$ kJ/mol and not the SWCNT growth. This is consistent with this rate-limiting step III being due to fullerene formation.

To test the statements above it appeared to be a straightforward check to determine the amount and distribution of fullerenes formed in synthesis experiments with and without catalyst (i.e., with and without SWCNT formation) under otherwise optimum SWCNT formation conditions. Generally, the use of transition metals as such is known to affect both the total amount of fullerenes as well as the fullerene distribution,[24] even when the transition metals do not catalyze SWCNT. We have verified this behavior in our experiments. Thus, under these circumstances, it is not possible to identify the fullerene

consumption process leading to the catalyzed formation of SWCNT from the experimental data.

3.2.3. Discussion of the Rate-Limiting Process II. As mentioned above, the fullerene studies have shown that for temperatures above 1000 °C[22] the slope describing fullerene formation in the Arrhenius plot levels off. Consequently, another thermally activated process with a different activation energy can become rate-limiting. This is the reason for the observation of a lower Arrhenius activation energy for argon and nitrogen above 1050 °C. As mentioned above, the SWCNT formation process can be considered to consist of a number of connected individual sub-processes. These individual steps should be executed in a certain sequence, whereby the growth of the nucleated SWCNT should be the final step. As follows from the analysis of the time scale of the individual gas-dynamic phenomena taking place during the ablation,[4,25] the SWCNT growth proceeds on much longer time scales than any other process (e.g., ablation, product condensation, thermalization of the ablation products) involved in the laser ablation cycle. Thus at some stage, a sub-process connected with this long-term growth will become the rate determining step.

At this point, a digression covering results published for the catalytical growth of carbon nanofibers is helpful. Reference 26 provides a comprehensive summary about the respective findings. As was demonstrated in ref 27, the activation energy of carbon filament growth exhibits a remarkable correlation with the activation energy for diffusion of carbon *through* a corresponding *solid* metal catalyst particle, measured directly by in-situ electron microscopy. The respective activation energies of carbon diffusion in solid Fe, Co, and Ni are comparable and lie within 126−148 kJ/mol.[26,27] On this basis, there is general agreement that this diffusion step of carbon through the submicron sized catalyst particle is the rate-determining step in the growth of carbon nanofibers.

Consequently, one might expect a similar thermally activated, rate-determining step for the metal particle catalyzed formation of SWCNT. Only, the activation energies of 30−40 kJ/mol under consideration here are much smaller than the above values. So, what are the possible reasons for this? In fact, upon closer inspection, these activation energies appear to be exceptionally low for any diffusion process through a solid particle. The key here is that the situation is different for a liquified particle.

In the production of bamboo-like hollow carbon structures by thermal decomposition of hydrocarbons[28] it was found that the metal catalyst-nanoparticles appeared to be molten during the synthesis. The same could be observed for the formation of multiwalled carbon nanotubes by CO disproportionation[29] and for the graphitization of amorphous carbon films.[30] All the structures mentioned above were catalyzed by metal catalyst nanoparticles at temperatures *several hundreds* of Kelvin below the equilibrium metal−carbon eutectic temperature. It could be determined that the liquid catalyst particles were highly supersaturated (containing up to 50% carbon).[30] An interrelation between the catalyst nanoparticle size and the temperature of the appearance of the molten state of the catalyst particles could be established.[29] The catalyst particle size distribution in our experiment, as estimated from TEM observations, was centered around 10−20 nm, which is similar to or smaller than those reported previously.[28−30] It is therefore reasonable to assume that the catalyst particles were molten in the temperature range between 800 and 1300 °C used in this work.

After this discussion of carbon nanofibers, we ask how does the SWCNT rate-limiting process II fit into this picture? It is now established from microgravity experiments in space[31] that

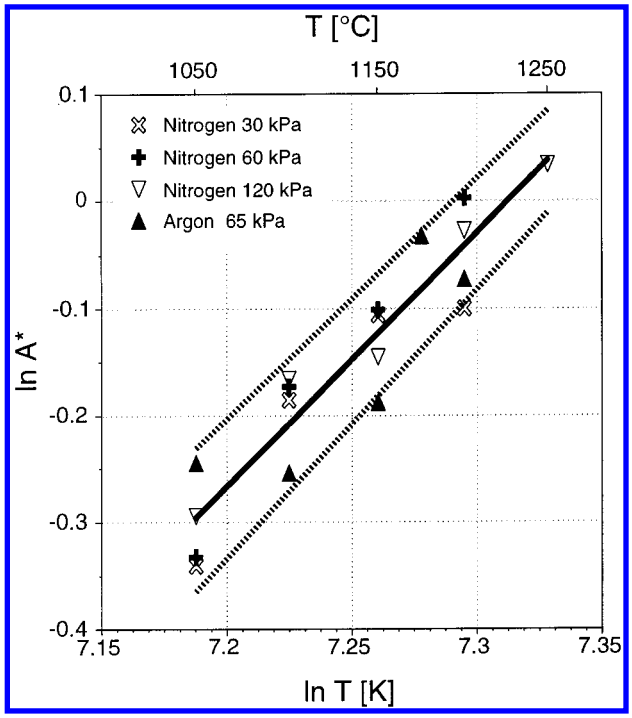

Figure 3. Log−log plot of the temperature dependence of the abundance data available for the rate-limiting process II. The data are taken from Figure 2c,d. A trend line (solid) is shown as well as lines (dotted) which serve as upper and lower bounds for this trend line derived from the experimental reproducibility $|\Delta A| = 0.05$. The slope of the trend line is 2.37.

diffusion in liquid metals follows a T^2-law. Thus, if the data describing process II originate from molten catalyst nanoparticles, one should observe a $D \propto T^2$ relation, and because process II is rate-limiting, $A^* \propto D \propto T^2$ should be obeyed. A plot of ln A^* vs ln T for all the group II data of Figure 2c,d is found in Figure 3. Shown are the data (symbols), a trend line (solid), and lines (dotted) which serve as upper and lower bounds for the trend line derived from the experimental reproducibility in $|\Delta A|$ of 0.05. It can clearly be seen from Figure 3 that the data fit well with the bounds. The bounds span up a range of power law coefficients between 2.25 and 2.5 with a value of 2.37 given by the central trend line.

It is necessary to realize that the given system is not a simple liquid but a eutectic system of carbon and a metallic solid solution: i.e., a binary or pseudobinary system. This means that, upon heating, the amount of liquid phase (and that of the coexisting solid phase) as well as their concentration might change. This would necessarily influence the temperature dependence of diffusion. In addition, it cannot be excluded that there is some interaction between the molecules in the liquid phase. These effects can be expected to lead to migration barriers in the liquid and resulting to a power law with T coefficients >2. Another well-known effect which increases the T power coefficient is convection in the liquid, which dominates over diffusion, although one might expect that for nanoparticles this effect is not pronounced. Influences of these types could easily explain the observed small shift of the slope seen in Figure 3 from an ideal T-square law to *slightly* larger T power coefficients. The data should thus be considered to provide strong evidence that the rate-limiting step II is due to the diffusion of carbon through *molten* catalyst particles.

3.2.4. High-Temperature Limit of the SWCNT Formation IV. Finally, the last rate limiting reaction step visible in the data of Figure 2c,d is the slightly pressure-dependent decrease of the

abundance for temperatures above that of the abundance maximum IV. Recently, by comparing different metal catalyst−carbon binary systems it could be shown that an analogous abundance decrease roughly coincides with the eutectic temperatures of the respective binary systems.[32] It was suggested that after melting of the catalyst particle no SWCNT can form. Upon a careful examination of the argon related data in Figure 2d (broken trend line), it appears that in fact the SWCNT detection limit coincides with the eutectics of bulk Ni−C and Co−C binary systems at ≈1320 °C. The existence of a temperature range for this limit might be attributed to small temperature fluctuation during the nanotube formation time scale.

On the other hand, such a simple explanation cannot be given for the pressure dependence of the abundance maxima shown in Figure 2a,b. To speculate, this could be due to a melting point reduction (and a similar reduction of the eutectic temperature of a binary system) at the particle surface which is well-established for extremely small particles.[33] Previously, we could show that SWCNT formation is favored for very small (<4 nm) metal catalyst nanoparticles;[7] thus, the assumption of a melting point reduction is reasonable. The surface tension of nanoparticles plays an essential role in this process. Any presence of gas molecules tends to reduce the surface tension, which diminishes the melting point reduction. This becomes more pronounced the more gas molecules are present. A higher pressure therefore shifts the onset of the melting to higher temperatures. This fits well with the observed shift of the SWCNT abundance maxima toward higher temperatures when higher pressures are used as is indeed seen in Figure 2a,b.

3.3. Undercooled Melt Mechanism for SWCNT Growth. The presented data are explicable within a scenario which extends the solid−liquid−solid mechanism for the growth of SWCNT we proposed in refs 34 and 35. In a nutshell, the mechanism we propose here is the following:

1. "Amorphous carbon" is dissolved in an extremely small metal catalyst particle. This results in the formation of a metastable melt at low temperatures. From the point of view of the "graphitic carbon"/metal system, the molten particle is both undercooled and supersaturated in carbon.

2. Once the metal particle becomes large enough it supports the nucleation of SWCNT (aided by fullerene seeds). A supersaturation-driven growth sets in.

3. "Amorphous carbon" dissolves steadily in the molten particle. The carbon atoms diffuse through a concentration gradient to the base of the continuously growing nanotube.

4. Any increase of the temperature above the eutectic temperature of the "graphitic carbon"/metal system *removes* the undercooling and a significant part of the carbon supersaturation from the molten catalyst particle. This reduces the driving force for SWCNT growth considerably.

Before going on to describe a model of the mechanism in more detail, we mention that there exist other suggestions as regards the SWCNT formation mechanism which involve liquid phases, such as those found in refs 36 and 37. However, none of these highlights the tight relation of the existence conditions of an undercooled melt with the SWCNT growth.

For our argumentation, we show the schematic phase-diagrams of the binary systems Me−g-C in Figure 4a and Me−"a-C" in Figure 4b (with Me being Ni, Co, and their alloys which form nearly ideal solid solutions; g-C being graphitic carbon; and "a-C" being "amorphous carbon"). In Figure 4c, both phase diagrams are plotted on top of one another, to highlight the differences between these two binary systems. Before going on, it should be noted that "a-C" is not a proper

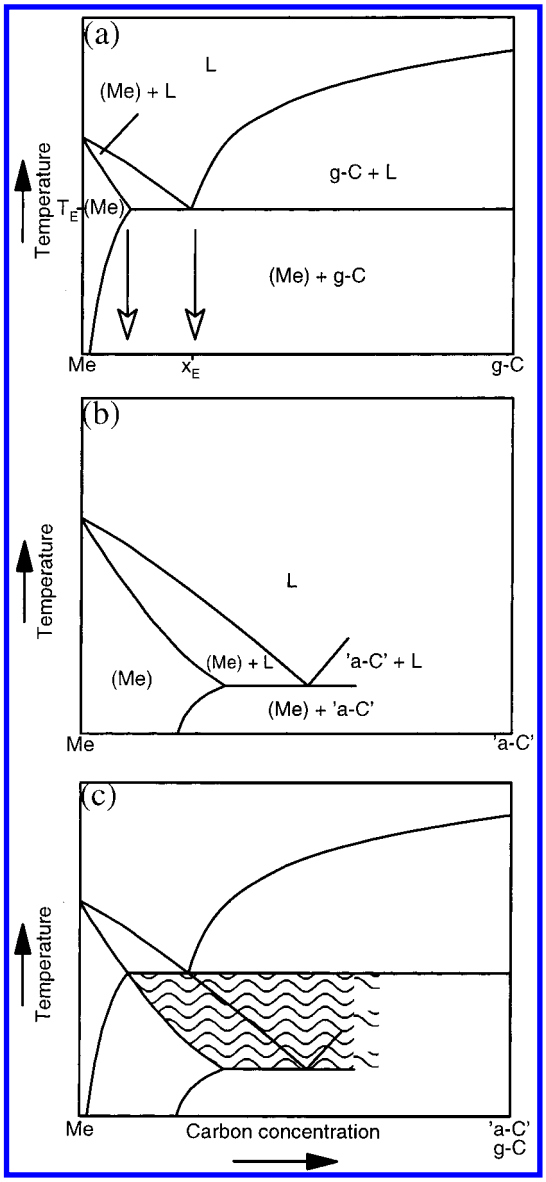

Figure 4. Schematic phase-diagrams of the binary systems Me−"a-C" (a) and Me−"a-C" (b). In (c), both phase-diagrams are copied above each other to highlight the differences between them. A shaded area in (c) indicates the existence range of a melt in the binary system Me−"a-C", which, from the point of view of the binary system Me−"a-C" represents a metastable, supersaturated, undercooled melt. The two arrows in (a) indicate the carbon content of the respective metal-containing phases with the highest possible carbon concentrations at temperatures slightly below (left arrow) and above the eutectic (right arrow). (Legend: Me = Ni, Co, or their binary alloys which form nearly ideal solid solutions; g-C = graphite, "a-C" = "amorphous carbon"; (Me) = solid solution of Me with carbon; L = liquid phase; T_E = eutectic temperature; x_E = eutectic composition).

phase with well defined properties but means rather a group of slightly different, more or less disordered, metastable phases. Consequently, the "a-C"-rich side of the phase diagram is not shown, and Figure 4,c should be considered to be "conceptual" rather than real. Nevertheless, for the binary system Me−"a-C", the following reported results are available which are incorporated in Figure 4b,c. For "a-C", higher values of the chemical potential compared to that of g-C can result in a higher solubility of carbon in the solid solution (Me). Solubilities of up to 50 at % determined from solubility experiments of amorphous carbon in nanosized Co particles are reported.[30] Accompanied with the extended solubility of carbon in Me is a shift of the eutectic to lower temperatures. Estimations have

been made of the lowest possible eutectic temperature in the binary system Me−"a-C".[29] They found for Me = Co values of ≈ 550 °C, which is far below that of the stable binary system Me−g-C (at ≈ 1320 °C). Metastable carbides of Me are known to be not present at temperatures higher than 395 °C.[29] An area in Figure 4c is shaded with horizontal wavy lines. This is the range of occurrence of a melt in the binary system Me−"a-C", which, from the point of view of the binary system Me−g-C is both *undercooled* and carbon *supersaturated*.

The reader might well ask how the binary system Me−"a-C"—in principle an unstable system—can exist, because M*e* is known to readily catalyze the conversion of "a-C" into g-C.[26] Indeed, this is one of the key issues for an understanding of the proposed mechanism of nanotube formation. One has to realize that we deal here with extremely small catalyst particles of only a few nm in size. The highly curved surface makes segregation processes of the necessarily highly strained graphitized material at the surface of a nanosized particle energetically unfavorable, i.e., they have a high activation energy barrier. In addition, the small size should not allow formation of crystallized, graphitic segregants at the particle surface if the respective particle size is below the critical size required for the formation of a stable graphitic nucleus, i.e., there exists a minimum particle size enabling the formation of graphitized material. It could indeed be shown that for the SWCNT formation this critical particle size is in the range of the SWCNT diameter.[7] Similarly, lower size limits for other graphitic structures might exist as well. Thus, these extremely small particles stabilize the existence of "a-C" so that in this context one might consider it to be metastable.

Due to ripening processes,[7] a catalyst particle grows and after some time it allows the heterogeneous nucleation of structures having a lower ΔG (higher degree of graphitization) than those originally dissolved. This would allow, in principle, the formation of graphite sheets as well as bamboo-shaped hollow carbons and multi- and single-walled tubes. Conformation considerations of possible structures at the metal particle/carbon interface can be found in ref 38. Partially or fully graphitized carbonaceous material (for example fullerenes) could act as a seed template, lowering the activation energy barrier for the heterogeneous nucleation of graphitized material from the metastable melt. A hypothesis regarding such a fullerene assisted nucleation of SWCNT has been published recently.[32]

Given the case that nucleation of SWCNT or other graphitized structures has taken place, the further reduction of the supersaturation of the undercooled melt is easily obtained by growth of the freshly nucleated, ordered graphitized structure. This results in a concentration gradient of carbon in the melt and thus results in a diffusive motion of carbon atoms through the catalyst particle to the base of the growing structure. The amorphous carbon in the surrounding of the catalyst particle acts as a feedstock: it further dissolves in the catalyst particle, keeping the particle supersaturated and molten and the diffusion process and growth of the graphitized structure running. The molten state allows a rather high diffusion velocity and therefore a high nanotube growth rate: nanotubes and nanotube bundles are commonly found to be apparently "endless" in electron microscopy observations despite an allowed nanotube growth time which is usually of the order of several hundreds of milliseconds in the laser evaporation approach (see, for example, refs 8 and 39). In contrast, carbon diffusion of carbon through solid catalyst nanoparticles is known to result in a growth rate of only a few nm/s (determined for the carbon nanofiber synthesis[26]).

Such a nucleation and growth of ordered structures from a melt is obviously limited to conditions for which an undercooling and a supersaturation can physically exist (a thermodynamic driving force has to be present) and also to conditions, for which the driving force is strong enough to overcome any kinetic inhibition effects. For example, any increase of the temperature of the binary system Me−"a-C" above the eutectic temperature of the binary system Me−g-C will remove the undercooling from the melt (Figure 4c). We assume now, that the carbon concentration in the supersaturated molten particle will be higher than the carbon concentration of the eutectic composition of the binary system Me−g-C. For this case, crossing the eutectic to higher temperature removes *most* of the carbon supersaturation from the melt. To outline this in more detail, a carbon supersaturated melt can decompose into two corresponding equilibrium phases: a carbon saturated (Me) solid solution and graphitic segregates *below* the eutectic, and into a carbon saturated melt L and graphitic segregates at temperatures *above*. The carbon content of these two carbon saturated phases (Me) and L in the vicinity of the eutectic is indicated by arrows in Figure 4a and is obviously different. The carbon content is significantly higher for the carbon saturated melt thus both the supersaturation and the driving force for the decomposition of a carbon supersaturated melt above the eutectic are *smaller*. The experimental results in ref 32 and also in this work show that there are no longer substantial quantities of SWCNT detected at temperatures above the eutectic of the binary system Me−g-C so that the driving force for the SWCNT growth can be considered to virtually disappear due to this loss of carbon supersaturation.

The reader will have noticed that the summary above reflects to some extent the experimental results of this work. The presented "undercooled melt" mechanism brings together apparently contradictory results, (1) that SWCNT formation is limited to temperatures below the eutectic temperature of the binary system of Co,Ni with graphite but (2) indications are found that point to a significant role of liquified ("molten") catalyst particles in the SWCNT formation process.

4. Summary

Four rate-limiting processes I−IV for the formation of single-wall carbon nanotubes (SWCNT) could be found by varying furnace temperature, gas type, and pressure in a pulsed-laser evaporation setup, by using a method based on optical absorption spectroscopy for the SWCNT soot characterization. One rate-limiting process accounts for *all* relevant gas-pressure dependencies in the SWCNT formation process, the three other rate determining steps that were identified are condensed phase bound.

(I) A single gas-kinetic process determines the transport conditions in the gas-space leading to well-defined conditions for optimal SWCNT abundance and to the existence of SWCNT formation limits. This was attributed to the quenching conditions possibly influencing the size of carbonaceous clusters. A quantitative expression could be given for this process that adequately describes the interplay of gas type, pressure, and temperature (see eq 2). The role of carrier gas molecules of different type is exclusively determined by their molecular cross section and weight.

This single gas-kinetic process is, except for a small pressure dependence of the eutectic temperature of the catalyst nanoparticles (rate-limiting process IV), the only process which was found to be influenced by gas-pressure variations. The derived quantitative expression enabled compensation for the influence

of the gas kinetic process, without which the determination of the nature of the other rate-limiting processes II + III would have been impossible.

(II) The rate-limiting process II follows roughly a *T*-square law, which is characteristic for diffusion processes through liquid metals. Consequently, process II was discussed in terms of diffusion processes of carbon through liquified metal catalyst nanoparticles.

(III) The rate-limiting process III is a thermally activated process. An Arrhenius activation energy range with $E_a \approx 70-90$ kJ/mol could be determined for this process. The activation energy and the temperature range in which this process dominates are fully consistent with process III being the footprint of the formation of higher fullerenes. This indicates an essential role of fullerenes in the formation of SWCNT.

(IV) It has been reported previously that SWCNT formation is limited to temperatures below the eutectic temperature of the pseudobinary system Ni,Co−graphite. This could be verified.

Rules for optimized SWCNT abundances can be derived from the rate-limiting processes described above. High temperatures are of advantage but this should be balanced by choosing an optimum ratio between $T^{3/2}$ and p for each carrier gas (see eq 2). To achieve a high-temperature synthesis of SWCNT, catalysts with high eutectic temperatures of their binary system with carbon should be chosen.

The presented data point unambiguously to an 'undercooled melt' mechanism for SWCNT growth. First, SWCNT formation is limited to temperatures below the eutectic temperature of the pseudobinary system Ni,Co−graphite. On the other hand, the data suggest an essential role of *molten* catalyst particles in the formation of SWCNT. In fact, such a liquified particle represents a supersaturated, undercooled melt from the point of view of the pseudobinary system Ni,Co−graphite. Such a metastable melt can form when "amorphous carbon" with its higher chemical potential compared to graphite dissolves in the catalyst particle which, on the other hand, is too small or too heavily curved to allow stable graphitic nuclei to form. Due to ripening processes,[7] the catalyst particle grows and after some time it allows the heterogeneous nucleation of SWCNT. Fullerenes can act as seed templates, lowering the activation barrier, after which supersaturation-driven growth of SWCNT reduces the degree of supersaturation of the undercooled melt. This results in a carbon concentration gradient through the melt and a carbon diffusion toward the base of the growing structure. Amorphous carbon from the environment surrounding the particle dissolves steadily into the particle, keeping the particle molten and supersaturated and the diffusion process and the SWCNT growth process running. Any increase of the temperature above the eutectic temperature of the pseudobinary system Ni,Co-graphite removes the undercooling and most of the carbon supersaturation from the melt so that the driving force for SWCNT growth virtually disappears.

Acknowledgment. This work was supported in part by the Saxonian Ministry of Science and Art (7531.50-03-823/5), the Deutsche Forschungsgemeinschaft (PO392/10-1/2 and FI439/8-1/2), and by the European Commission through the IST-FET "Nanotechnology Information Devices" initiative (IST-1999-10593 "SATURN"). We are grateful to A. E. Tselev, J. Drechsel, K. Müller, and H. Zöller for experimental assistance and to L. C. Ciacchi for fruitful discussions.

References and Notes

(1) Dresselhaus, M. S.; Dresselhaus, G.; Eklund, P. C. *Science of Fullerenes and Carbon Nanotubes*; Academic Press: San Diego, 1996.

(2) Dresselhaus, M. S.; Dresselhaus, G.; Avouris, Ph., Eds. *Carbon Nanotubes−Synthesis, Structure, Properties, and Applications*; Springer: Berlin, 2001.

(3) Terrones, M., Tsu, W. K., Kroto, H. W., Walton, D. R. M., Hirsch, A., Eds. *Topics in Current Chemistry*; Springer: Berlin 1999; Vol. 199, p 189.

(4) Gorbunov, A. A.; Friedlein, R.; Jost, O.; Golden, M. S.; Fink, J.; Pompe, W. *Appl. Phys. A* **1999**, *69*, S593.

(5) Sen, R.; Ohtsuka, Y.; Ishigaki, T.; Kasuya, D.; Suzuki, S.; Kataura, H.; Achiba, Y. *Chem. Phys. Lett.* **2000**, *332*, 467.

(6) Kokai, F.; Takahashi, K.; Yudasaka, M.; Iijima, S. *J. Phys. Chem. B* **2000**, *104*, 6777.

(7) Jost, O.; Gorbunov, A. A.; Möller, J.; Pompe, W.; Graff, A.; Friedlein, R.; Liu, X.; Golden, M. S.; Fink, *J. Chem. Phys. Lett.* **2001**, *339*, 297.

(8) Rinzler, A. G.; Liu, J.; Dai, H.; Huffman, C. B.; Rodriguez-Macias, F.; Boul, P. J.; Lu, A. H.; Heymann, D.; Colbert, D. T.; Lee, R. S.; Fischer, J. E.; Rao, A. M.; Eklund, P. C.; Smalley, R. E. *Appl. Phys. A* **1998**, *67*, 29.

(9) Bandow, S.; Asaka, S.; Saito, Y.; Rao, A. M.; Grigorian, L.; Richter, E.; Eklund, P. C. *Phys. Rev. Lett.* **1998**, *80*, 3779.

(10) Takizawa, M.; Bandow, S.; Torii, T.; Iijima, S. *Chem. Phys. Lett.* **1998**, *302*, 146.

(11) Laplaze, D.; Bernier, P.; Maser, W. K.; Flamant, G.; Guillard, T.; Loiseau, A. *Carbon*, **1998**, *36*, 685.

(12) Journet, C., Lamy de la Chapelle, M., Loiseau, A., Fischer, J. E., Lefrant, S., Bernier, P., Kuzmany, H.; Fink, J., Mehring, M., Roth, S., Eds. *Proceedings of the 13th International Winterschool on Electronic Properties of Novel Materials*; American Institute of Physics: New York, 1999; p 292.

(13) Yudasaka, M.; Kokai, F.; Takahashi, K.; Yamada, R.; Sensui, N.; Ichihashi, T.; Iijima, S. *J. Phys. Chem. B* **1999**, *103*, 3576.

(14) Yudasaka, M.; Komatsu, T.; Ichihashi, T.; Achiba, Y.; Iijima, S. *J. Phys. Chem. B* **1998**, *102*, 4892.

(15) Kataura, H.; Kumazawa, Y.; Maniwa, Y.; Umezu, I.; Suzuki, S.; Ohtsuka, Y.; Achiba, Y. *Synth. Met.* **1999**, *100*, 2555.

(16) Pichler, T.; Golden, M. S.; Knupfer, M.; Fink, J.; Rinzler, A. G.; Smalley, R. E. *Phys. Rev. Lett.* **1998**, *80*, 4729.

(17) Jost, O.; Pichler, T.; Friedlein, R.; Gorbunov, A. A.; Knupfer, M.; Reibold, M.; Bauer, H.-D.; Dunsch, L.; Golden, M. S.; Fink, J.; Pompe, W. *Appl. Phys. Lett.* **1999**, *75*, 2217.

(18) Zhang, Y.; Gu, H.; Iijima, S. *Appl. Phys. Lett.* **1998**, *73*, 3827.

(19) Munoz, E.; Maser, W. K.; Benito, A. M.; Martinez, M. T.; de la Fuente, G. F.; Maniette, Y.; Righi, A.; Anglaret, E.; Sauvajol, J. L. *Carbon* **2000**, *38*, 1445.

(20) Gamaly, E. G.; Rode, A. V.; Maser, W. K.; Munoz, E.; Benito, A. M.; Martinez, M. T.; de la Fuente, G. F. *Appl. Phys. A* **2000**, *70*, 161.

(21) Zhang, S.; Iijima, S. *Appl. Phys. Lett.* **1999**, *75*, 3087.

(22) Kasuya, D.; Ishigaki, T.; Suganuma, T.; Ohtsuka, Y.; Suzuki, S.; Shiromaru, H.; Achiba, Y.; Wakabayashi, T. *Eur. Phys. J. D* **1999**, *9*, 355.

(23) Ishigaki, T.; Suzuki, S.; Kataura, H.; Krätschmer, W.; Achiba, Y. *Appl. Phys. A* **2000**, *70*, 121.

(24) Seraphin, S.; Zhou, D.; Jiao, J.; Minke, M. A.; Wang, S.; Yadav, T.; Withers, J. C. *Chem. Phys. Lett.* **1994**, *217*, 191.

(25) Puretzky, A. A.; Geohegan, D. B.; Fan, X.; Pennycook, S. J. *Appl. Phys. A* **2000**, *70*, 153.

(26) Rodriguez, N. M. *J. Mater. Res.* **1998**, *8*, 3233.

(27) Baker, R. T. K.; Harris, P. S.; Thomas, R. B.; Waite, R. J. J. *Catalysis* **1973**, *30*, 86.

(28) Li, Y.; Chen, J.; Ma, Y.; Zhao, J.; Qin, Y.; Chang, L. *Chem. Commun.* **1999**, 1140.

(29) Khassin, A. A.; Yurieva, T. M.; Zaikovskii, V. I.; Parmon, V. N. *React. Kinet. Catal. Lett.* **1998**, *64*, 63.

(30) Krivoruchko, O. P.; Zaikovskii, V. I. *Mendeleev Commun.* **1998**, *3*, 97.

(31) Mathiak, G.; Griesche, A.; Kraatz, K. H.; Frohberg, G. *J. Non-Cryst. Solids* **1996**, *207*, 412.

(32) Kataura, H.; Kumazawa, Y.; Maniwa, Y.; Ohtsuka, Y.; Sen, R.; Suzuki, S.; Achiba, Y. *Carbon* **2000**, *38*, 1691.

(33) Schmidt, M.; Kusche, R.; Kronmüller, W.; v. Issendorff, B.; Haberland, H. *Phys. Rev. Lett.* **1997**, *79*, 99.

(34) Gorbunov, A. A.; Graff, A.; Jost, O.; Pompe, W. In *Proceedings of SPIE*; Libenson, N. M., Ed.; The International Society for Optical Engineering: Bellingham, 2001; Vol. 4423, p 217.

(35) Gorbunov, A. A.; Jost, O.; Pompe, W.; Graff, A. *Carbon* **2002**, *40*, 113.

(36) Kanzow, H.; Ding, A. *Phys. Rev. B* **1999**, *60*, 11180.

(37) Loiseau, A.; Willaime, F. *Appl. Surf. Sci.* **2000**, *164*, 227.

(38) Maiti, A.; Brabec, C. J.; Bernholc, *J. Phys. Rev. B* **1997**, *55*, R6097.

(39) Guo, T.; Nikolaev, P.; Thess, A. Colbert, D. T.; Smalley, R. E. *Chem. Phys. Lett.* **1995**, *243*, 49.